

# Evaluation of Fatigue Damage in Adhesive Bonding: Part 1: Bulk Adhesive

M. M. Abdel Wahab<sup>a,\*</sup>, I. Hilmy<sup>b</sup>, I. A. Ashcroft<sup>c</sup> and A. D. Crocombe<sup>b</sup>

<sup>a</sup> Department of Mechanical Construction and Production, Faculty of Engineering,  
Ghent University, B-9000 Gent, Belgium

<sup>b</sup> Faculty of Engineering and Physical Sciences, University of Surrey, Guildford,  
Surrey, GU2 5XH, UK

<sup>c</sup> Department of Mechanical Engineering, Loughborough, Leicestershire, LE11 3TU, UK

Received in final form 9 October 2008; revised 2 November 2008; accepted 11 August 2009

---

## Abstract

The measurement of fatigue damage in adhesive bonding has been investigated. Bulk adhesive was used in this study for two reasons: the stress distribution of adhesives in bulk is simpler to investigate than adhesives in joints; and the specimen dimensions met fatigue test standards. Bulk adhesive was made from a film type of epoxy resin. In general, the characteristics and the behaviour of bulk adhesive may differ from adhesive in joint because of the presence of voids and the constraints imposed by the substrates. Low cycle fatigue tests with a load amplitude ratio of 0.1 at a frequency of 5 Hz were performed to determine the damage as a function of the number of cycles. Damage curves, i.e., the evolution of the damage variable as a function of number of cycles, were derived and plotted using an isotropic damage equation. Damage was evaluated using the decrease of stress range during the lifecycles of a constant displacement amplitude test. It was found that the damage curves were well fitted by a low cycle, fatigue damage evolution law equation. This equation was derived from a dissipation potential function. Curve fitting was performed using the robust least square technique rather than ordinary linear least square technique because damage curves have extreme points (usually near the failure point). It was found that the fitting process would not converge for adhesive fractures at high cycle values ( $N_f > 9000$ ). Two damage constants  $A$  and  $\beta$  were found from the fitting process. Each fatigue set of data, at a certain level of von-Mises stress range for the undamaged state or at the stabilized hardened state, ( $\Delta\sigma_{eq}^*$ ), had a different set of damage parameters  $A$  and  $\beta$ . Linear regression of these points was used to express  $A$  and  $\beta$  as a function of  $\Delta\sigma_{eq}^*$ . Using these expressions, damage curves for different levels of  $\Delta\sigma_{eq}^*$  could be predicted.

© Koninklijke Brill NV, Leiden, 2010

## Keywords

Continuum damage mechanics, damage parameters, low cycle fatigue, bulk adhesive, crack initiation, life-time prediction

---

\* To whom correspondence should be addressed. E-mail: magd.wahab@ugent.be

## 1. Introduction

Adhesive bonding is by definition, the process of joining two parts/structures using non-metallic material (the adhesive) [1]. This bonding undergoes a chemical and physical hardening reaction causing the parts to be jointed together through surface adherence (adhesion) and internal strength (cohesion). For most adhesive systems, the adhesive region is the weakest part because the attractive forces between the adhesive and the substrate (adhesion) are stronger than the forces within the adhesive layer (cohesion). Usually the internal strength of the substrate and the adhesive can be controlled. The strength of substrate can be controlled during its manufacture and the strength of the adhesive can be controlled by adjusting the heating process and the curing time. But if the area of contact (interface) is the weakest part, because of imperfect contact, then the joint strength will be weak. As a result, failure at low loadings or due to non-uniform strength along bondlines, will take place.

Many mechanical failure modes might take place in adhesive systems. This failure can happen to a system with simple to complex configurations. It is estimated that between 50–90% of the failure is caused by fatigue [2].

In 1870, Wohler as cited by Blaum [3] was the first researcher to systematically investigate fatigue; his research was based on train chassis. He investigated material behaviour under constant loading amplitude. Subsequently, structural behaviour under a specific load for various different materials has been investigated, both experimentally and numerically. Fatigue crack growth is understood to some extent, but the phenomenon of crack initiation is not yet fully understood.

Low cycle fatigue failure has the following characteristics: the structure suffers high load; lives are relatively short; and significant plastic straining takes place. The failure caused by a low cycle fatigue load takes place in structures subjected to a heavy load. This load induces irreversible strain at a micro-scale or macro-scale level. The damage accumulated in a structure will reach the point of initiation and propagation of cracks. A cycle is usually defined as the interval between two service times. The number of cycles leading to failure ( $N_f$ ) is relatively small. Lemaitre and Desmorat [4] have categorized the classification of low cycle fatigue as follows:

1. The value of  $N_f$  lies between 10–100 for aerospace rockets or metal formed by forging. Stresses are between  $\sigma_u > \sigma > \sigma_y$ , where  $\sigma_u$  is the ultimate stress and  $\sigma_y$  is the yield stress.
2. The value of  $N_f$  lies between 100–1000 for thermal or nuclear power plants or chemical plants. Stresses are slightly larger than the yield stress.
3. The value of  $N_f$  lies between 1000–10 000 for aircraft engines or car engines where stresses induce plastic strain with magnitudes approaching  $\varepsilon_p \approx \sigma_y/E$ , where  $\varepsilon_p$  is the plastic strain and  $E$  is Young's modulus.

The damage model presented in this paper makes use of a low cycle fatigue model, which is based on the accumulation of plastic strains. The low cycle fatigue

damage model is mainly considered when the plastic strain is high enough to be measured. In such a case, the stresses should be higher than the yield stress of the material and the number of cycles leading to failure, corresponds to less than or equal to 10 000 cycles. If the number of cycles to failure is too high, say more than 100 000 cycles, the plastic strain is of micro-size and not measurable and, therefore, the low cycle fatigue model is not applicable. It is worth mentioning that because structural adhesive joints always contain stress singularity points, the stresses are singular, i.e., exceed the elastic limit and plastic zones form around these points. Therefore, a low cycle fatigue damage model is always suitable for adhesive joints regardless of the number of cycles leading to failure.

The basic characteristic of low cycle fatigue is based on the Coffin–Manson equation as described in [5]. Figure 1 shows a typical Coffin–Manson Curve. An approximate version of the Coffin–Manson equation is given by:

$$N_f = \left( \frac{C_{mc}}{\Delta \varepsilon_p} \right)^\gamma, \tag{1}$$

where  $C_{mc}$  and  $\gamma$  are material parameters;  $C_{mc}$  depends on temperature and  $\gamma$  is close to 2 regardless the type of material and temperature. The total strain amplitude can be calculated as follows [6]:

$$\frac{\Delta \varepsilon_T}{2} = \frac{\Delta \varepsilon_e}{2} + \frac{\Delta \varepsilon_p}{2} = \frac{\sigma'_f}{E} (2N_f)^b + \varepsilon'_f (2N_f)^c, \tag{2}$$

where  $\frac{\Delta \varepsilon_e}{2}$  is the elastic strain amplitude;  $\frac{\Delta \varepsilon_p}{2}$ , the plastic strain amplitude;  $\sigma'_f$ , the fatigue strength coefficient, defined by the stress intercept at one load reversal (see Fig. 1);  $\varepsilon'_f$ , the fatigue ductility coefficient, defined by the strain intercept at one load

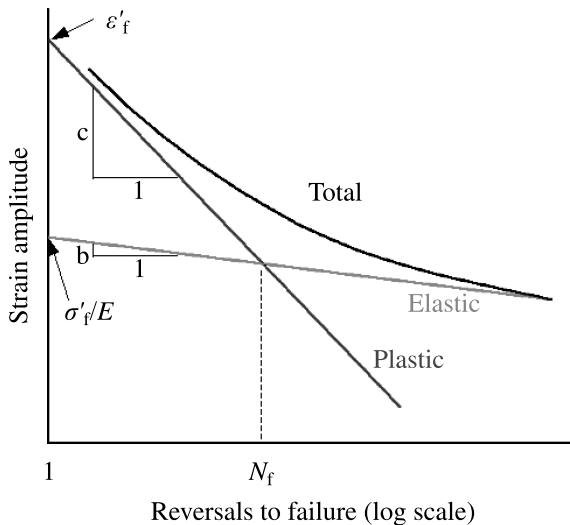


Figure 1. Typical joint lifetime according to Coffin–Manson’s equation, adapted from Onem [6].

reversal;  $2N_f$ , the total number of reversals to failure; and  $b$  and  $c$  are the fatigue ductility exponents (material properties).

Nowadays, there is still a debate among researchers about which mechanism contributes most to the lifetime of a joint — crack initiation or crack propagation. The problem is that it is not easy to prove which mechanism is dominant. Different ratios of crack initiation to crack propagation lifetimes can be found depending on how crack initiation is defined, measured and what techniques are used in order to monitor crack propagation. Researchers have also found that modifying the geometry and fracture property may lead to different results.

There are two common techniques used to observe damage and cracks in adhesive joints, namely: video microscopy; and the back–face strain technique. Courta *et al.* [7] used transparent polymethylmethacrylate adherends (PMA) so that the crack propagation inside joints could be observed visually using a video camera. It was concluded that crack initiation dominated the life time of the joint before it failed. Harris and Fay [8] used video microscopy to observe the side of single lap joints used in automotive applications and to identify crack initiation. Again, it was found that fatigue lifetime was dominated by crack initiation. A back–face strain technique has been used and extended by several researchers: e.g., Zhang *et al.* [9], Imanaka *et al.* [10] and Crocombe *et al.* [11].

Crocombe *et al.* [11] concluded that for adhesive joints, involving a fillet, more than 50% of the lifetime was dominated by crack initiation. When the fillet was removed, the joint lifetime decreased significantly and the crack initiation period reduced to almost zero; the ratio of crack initiation lifetime to propagation lifetime increased as the load level decreased.

Marcadon *et al.* [12] has studied the durability of a vinyl ester adhesive T-joint used in the structural part of a ship. After careful observation of the cracking mechanism, it was found that the crack propagation of T-joints dominated about two third of the fatigue failure lifetime. Using a back–face strain method, Zhang *et al.* [9] found that the ratio of crack initiation to crack propagation lifetimes of single lap joints was not constant.

There have been cases where different experimental results for crack initiation have been found for the same adhesive/substrate joint system. For example, for the same adhesive system, Crocombe [13] and Curley *et al.* [14] found that the crack initiation phase was less than 60% and 15%, respectively. For this test, Curley *et al.* [14] used a specimen with a spew-fillet and the results were observed using a back–face strain method of the same dimensions and size. Crocombe used a specimen with a controlled fillet and observed crack initiation using video microscopy [13].

The main aim of the first part of this paper is to measure crack initiation damage parameters of adhesives using bulk adhesive test specimens. The damage parameters, which are function of the stress level in the adhesives, were determined by fitting the experimental data to a damage evolution law. In the second part of this paper, the technique is further extended and applied to the adhesives in a single lap

joint, in order to include the effect of the triaxial function on the damage parameters and the prediction of crack initiation lifetime.

## 2. Experimental Set-up

Bulk adhesive specimens were used in this experiment as a first step in order to determine the fatigue damage parameters. It has the advantage that the interpretation of stress–strain data of the bulk adhesive is easier than it is for adhesives in joints. Bulk adhesive has a simpler stress distribution because of the absence of substrates [15]. The specimens were made from epoxy resin, FM-73 film adhesive, supplied by Cytec™. Epoxy resins are a class of versatile thermosetting polymers and are extensively used in structural adhesives for polymer composites. This is because of their high strength, low creep, very low cure shrinkage, excellent resistance to corrosion, good adhesion to many substrates and appropriate electrical properties [16].

The placement of bulk adhesive along with its support apparatus is shown in Fig. 2. The function of the weight is to give pressure to the upper glass plate, which will be transferred to bulk adhesive. The use of a reference thickness plate is to stop the reduction in adhesive thickness during the heating and pressurising processes. The stopper is used to avoid the sliding movement of the upper glass. If sliding does take place, it will cause the adhesive to tear.

There are two ways in which air can be trapped inside the bulk adhesive: during the film manufacturing process; and during the bulk adhesive manufacturing process. The higher number of stacking layers, the greater is the possibility of trapping air bubbles. This phenomenon is shown in Fig. 3.

To minimize the chance of air bubble formation, pressure was applied. In the early stages of the investigation, after every four layers, pressure was applied using

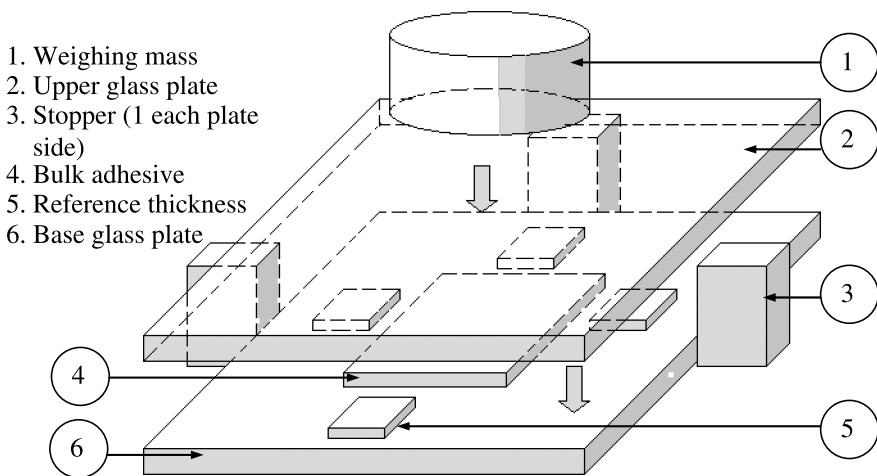


**Figure 2.** Specimen placement used to perform the heating process.

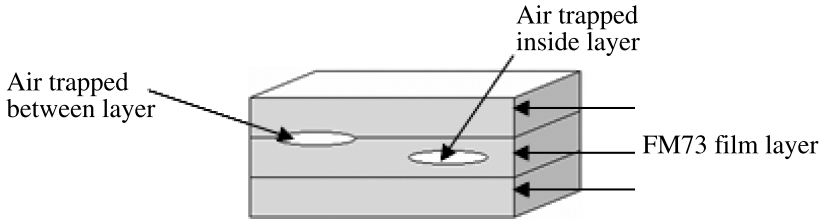


**Figure 3.** Trapped air bubble inside bulk adhesives.

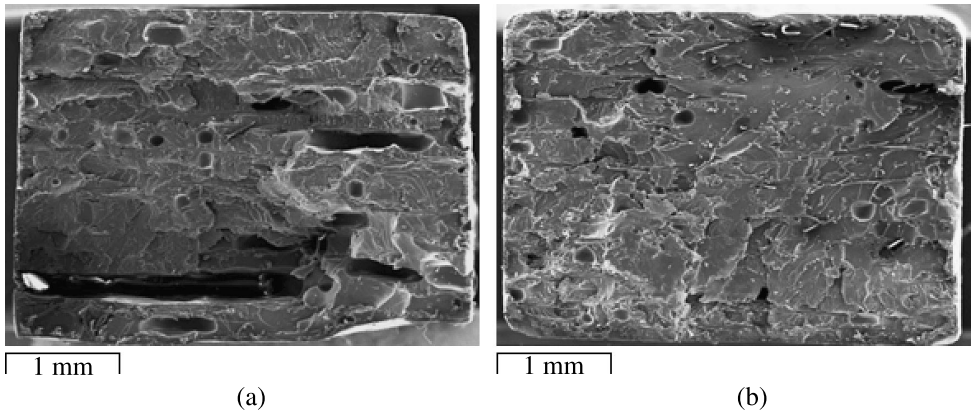


**Figure 4.** Fractured surface of FM-73 bulk adhesive; (a) before, (b) after manufacturing improvement.

a pressure roller. The result is shown in Fig. 4(a) indicating the presence of voids. To improve the quality of bulk adhesive, increased pressure was applied after stacking every single layer. The result is shown in Fig. 3(b); again showing voids in spite of the increased pressure. Voids act as stress raisers or stress concentrators and in that way promote premature failure. It was concluded that the real bulk adhesive strength might differ from the adhesive model in the joint, because the number of voids present might be different.

Two types of experiments were performed: tensile tests; and fatigue tests. The tensile tests used the *Instron 5500R, frame 6025* machine which had the following characteristics: maximum load range was 100 kN; cross-head displacement rate was from 0.001 to 1000 mm/minute; and it was controlled by MERLIN software [17]. The fatigue tests were carried out using an *Instron 8511 Test System*. The model 8511 is a compact servo-hydraulic material testing system designed for linear dynamic test forces for specimens from a wide range of materials. This machine was controlled by built-in software called MAX. Figure 5 shows the Instron 8511 machine and the test set-up. Figure 6(a) shows a picture of the bulk adhesive test specimens and Fig. 6(b) shows its dimensions. The specimen was machined in the mechanical workshop of the University of Surrey.

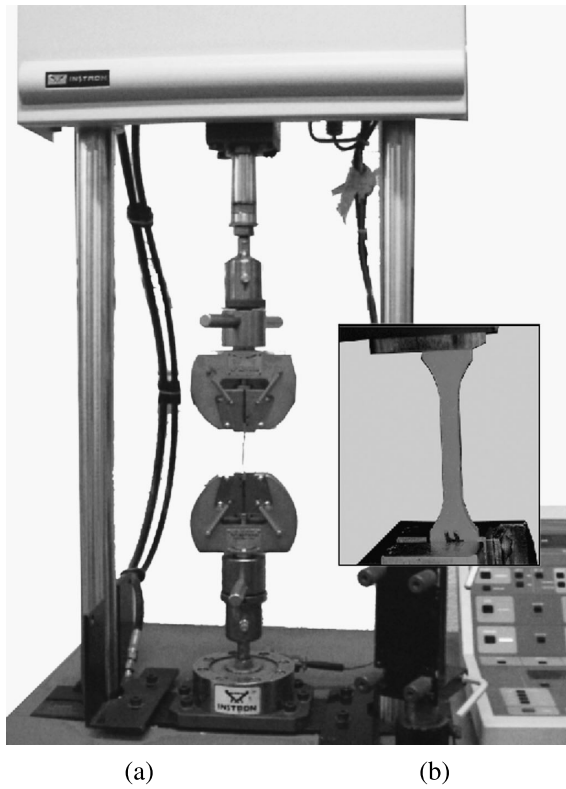


**Figure 5.** Instron 8511 Machine; (a) front view, (b) main component.

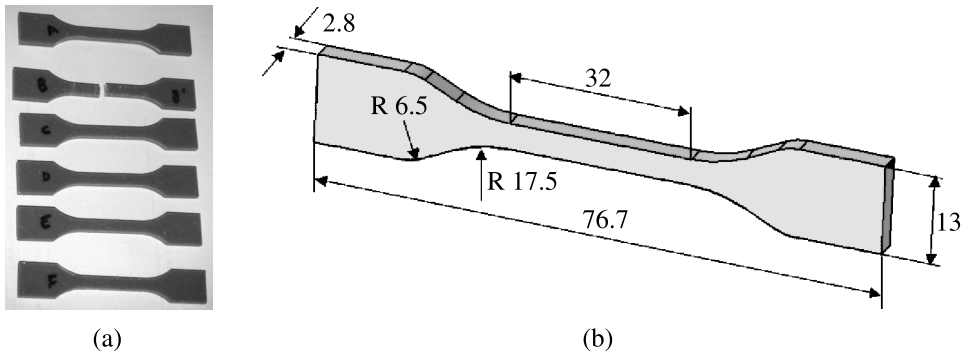


**Figure 6.** (a) Test specimen and (b) dimensions (in mm).

To obtain the equivalent stress on the bulk adhesive as a function of time or cycles, a low cycle fatigue (LCF)-strain based test was performed. The triangular strain shape was chosen because of its linear shape. Although the turning point was sharp, the effect was small because the test was carried out at low frequency. The

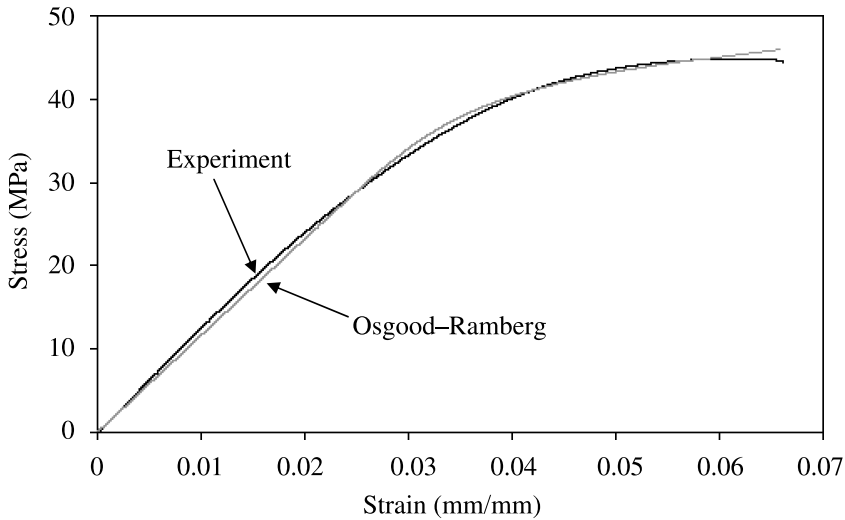


**Figure 7.** Curve fitting of stress–strain curve of bulk adhesive from tensile test.

minimum displacement was 0.24 mm, the maximum displacement was 1.4 mm and the test frequency was 5 Hz.

The tensile test was performed in order to obtain the material parameters needed for the damage evolution formula and finite element analysis. The tests were performed by controlling the extension (extension rate = 0.016 mm/s) of the specimen up to the failure point, while recording the load. Direct results of load as a function of extension were obtained. This curve was then converted to an engineering stress–strain curve by dividing the force and the extension by the cross-sectional area and the initial length of specimen, respectively. The Ramberg–Osgood formula equation was fitted to the stress–strain data [18]. The curve fitting process was performed using the facility, ‘Cftool’ provided by MATLAB. The results are shown in Fig. 7. From the curve fitting procedure, the material properties of the bulk adhesive were found to be:  $E = 1160 \text{ N/mm}^2$ ;  $K = 61.437 \text{ N/mm}^2$ ; and  $m = 0.08$ , where  $E$  is Young’s modulus and  $K$  and  $m$  are Ramberg–Osgood parameters.

Several low cycles fatigue tests were performed. Some specimens were eliminated for inconsistency results. This was because the specimen had voids greater than the average. The results are shown in Fig. 8 as the strain range  $\Delta\varepsilon$  (%) versus the number of cycles to failure,  $N_f$ , in a logarithmic scale — this being the Manson–Coffin curve form.

In Fig. 9, the measured load as a function of number of cycles is given. It shows the decrease in maximum and minimum loads after each cycle. A decrease in stress range indicates a degradation of stiffness during its lifetime. This is a characteristic of the constant strain (or displacement) amplitude fatigue test.

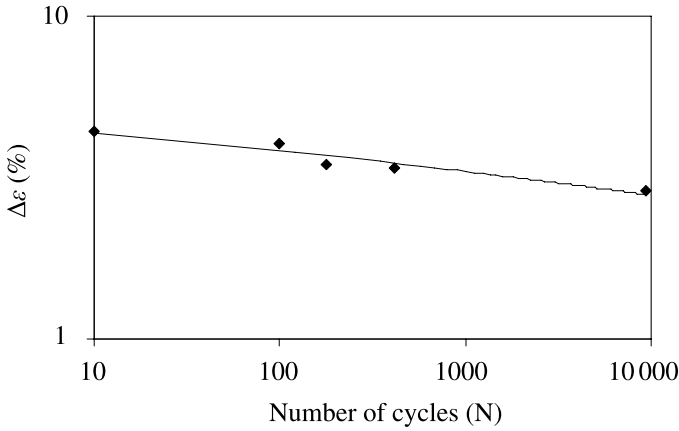


Figure 8. Strain range  $\Delta\epsilon$  function of  $\log(N_f)$ .

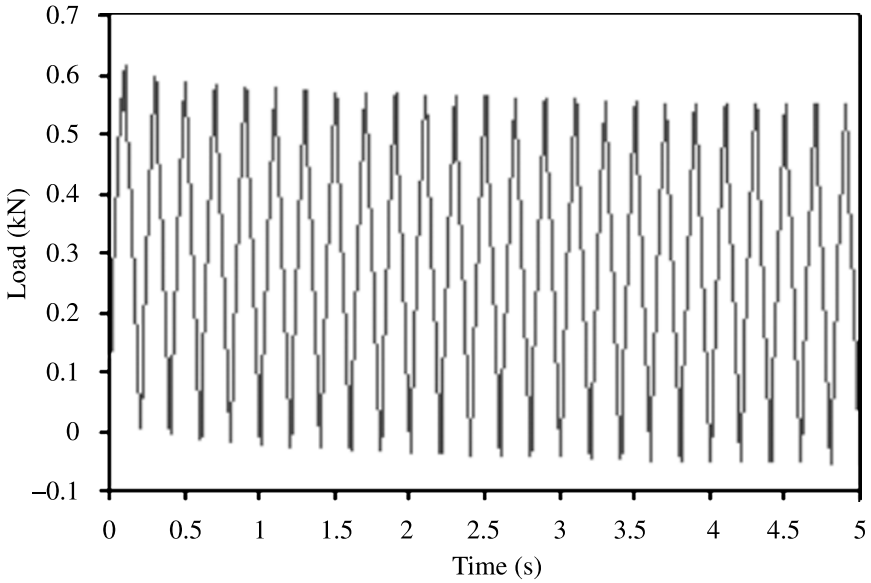
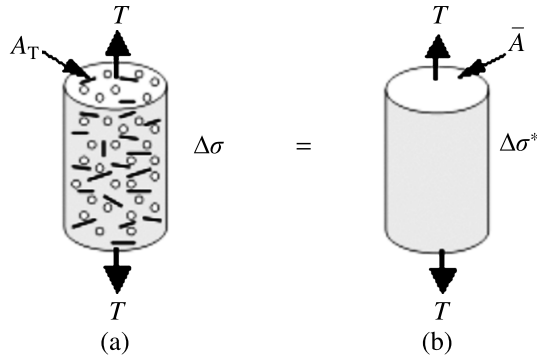


Figure 9. Sample of constant strain amplitude fatigue raw data.

### 3. Damage Measurement Based on Stress Degradation

Stress degradation occurs during a strain-based controlled test. To obtain the damage variable ( $D$ ) as a function of number of cycles, applied stress range and triaxiality, one should develop a damage equation based on thermodynamics principles as developed by Wahab *et al.* [19], i.e.:

$$D = 1 - [1 - A(\beta + m + 1)(\Delta\sigma_{eq})^{\beta+m} R_V^{\beta/2} N]^{1/(\beta+m+1)}, \quad (3)$$



**Figure 10.** Two equivalent damage models: (a) bar with voids and cracks and (b) bar without voids and cracks.

where  $D$  is the damage variable,  $N$  is the number of cycles,  $\Delta\sigma_{eq}$  the range of von-Mises stress,  $R_V$  the triaxiality function,  $m$  the power constant in Ramberg–Osgood equation, and  $A$  and  $\beta$  are damage parameters to be determined experimentally. It should be noted that  $\Delta\sigma_{eq}$  is the applied stress range at the beginning of the fatigue cycles. Thus, in case of the constant displacement amplitude test, the stresses decreased as function of number of cycles and  $\Delta\sigma_{eq}$  should be replaced by  $\Delta\sigma_{eq}^*$ , which is the von-Mises stress range for virgin material or at the stabilized hardened state (see later equation (9)).

Figure 10 shows the model proposed by Voyiadjis and Kattan [20]. Two equivalent models of a damaged bar have been compared. The first bar has cracks and micro-voids (Fig. 10(a)), while the second one has neither cracks nor voids, i.e., voids and cracks are removed from the first bar (Fig. 10(b)). The second bar has a cross-sectional area  $\bar{A} = A_T - A_D$  (where  $A_T$  is the total cross-sectional area and  $A_D$  is the crack and micro-void cross-sectional area), which means the area has been reduced after the removal of voids and micro-cracks. A uniaxial fatigue load range  $\Delta T$  is applied to both rods. The stress range in the damaged state is denoted by  $\Delta\sigma$ , while the stress range in the undamaged state is denoted by  $\Delta\sigma^*$ . If the same fatigue load range  $\Delta T$  is applied to both damaged and undamaged models, it can be calculated as:

$$\Delta T = \Delta\sigma A_T, \quad \text{for first bar (with damage),} \tag{4}$$

$$\Delta T = \Delta\sigma^* \bar{A} = \Delta\sigma^* (A_T - A_D), \quad \text{for the second bar (without damage).} \tag{5}$$

Since  $\Delta T$  from equation (4) is equal to  $\Delta T$  from equation (5), i.e.:

$$\Delta\sigma A_T = \Delta\sigma^* (A_T - A_D). \tag{6}$$

Equation (6) rearranges as:

$$\Delta\sigma = \Delta\sigma^* \left( 1 - \frac{A_D}{A_T} \right). \tag{7}$$

Substituting  $A_D/A_T$  with  $D$ , equation (7) becomes:

$$\Delta\sigma = \Delta\sigma^*(1 - D). \quad (8)$$

Finally the damage variable  $D$ , is defined as:

$$D = 1 - \frac{\Delta\sigma}{\Delta\sigma^*}. \quad (9)$$

In order to determine the damage parameters,  $A$  and  $\beta$ , equation (3) is simplified in a polynomial form, with two constants  $C_1$  and  $C_2$  defined as:

$$(\beta + m + 1)A(\Delta\sigma_{eq})^{\beta+m}R_V^{\beta/2} = C_1, \quad (10)$$

where  $\beta + m + 1 = C_2$ . Equation (3) becomes:

$$D = 1 - [1 - C_1N]^{1/C_2} \quad (11)$$

and re-arranging equation (11) gives:

$$1 - D = [1 - C_1N]^{1/C_2}. \quad (12)$$

Let  $1 - D = D_m$  and powered both sides by  $C_2$ , leads to:

$$D_m^{C_2} = 1 - C_1N. \quad (13)$$

And re-writing equation (13) as:

$$\frac{1}{C_1}D_m^{C_2} - \frac{1}{C_1} = -N. \quad (14)$$

If  $1/C_1 = K_1$ , a simpler form of the damage equation is obtained:

$$N = K_1 - K_1D_m^{C_2}, \quad (15)$$

with  $K_1$  and  $C_2$  values obtained by fitting equation (15) to the damage experimental data. The fitting process was performed using ‘cftool’ command provided in MATLAB. This command uses a trust-region algorithm, which is an improvement of Levenberg–Marquardt algorithm and implements the least absolute residuals (LAR) method. Using the LAR method for the fitting, in this case is better than using the least square (LS) technique, because LS is more sensitive for extreme values (outliers) [21]. With the trust-region algorithm, non-linear problems can be solved more efficiently when compared to other algorithms. The MATLAB code for curve fitting of equation (15) to experimental data is given in Appendix A.

Referring to equation (3), since the damage calculation only needs maximum and minimum load values (to calculate the von-Mises stress range and the average triaxiality function), these values can be extracted from the fatigue raw data. To extract the required data, an algorithm was implemented in MATLAB. The result of fatigue data extraction is shown in Fig. 11. The curve is formed from peak points connected from one cycle to the next cycle. The decrease in maximum or minimum loads is made clear after converting the raw data.

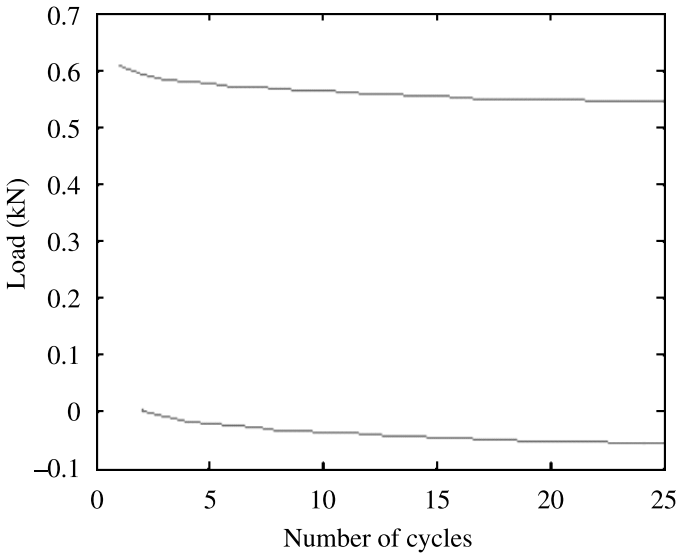


**Figure 11.** Extracted data from raw data using MATLAB code for  $\Delta\sigma_{\text{eq}}^* = 43.88$  MPa.

The advantage of this data extraction process is that huge amounts of data obtained from fatigue test can be significantly reduced. Computing time can also be reduced. The next step was to calculate the difference between maximum and minimum loads. This value is called  $\Delta L$  (fatigue load range at a certain damage state) corresponding to  $\Delta\sigma_{\text{eq}}$  (von-Mises stress range at a certain damage state).

Using linear regression of the stabilized region, which is intersected with the load axis,  $\Delta L^*$  (fatigue load range at undamaged state or at the stabilized hardened state as shown in Fig. 12) can be determined. From equation (9), since the total cross-sectional area is constant during its lifecycle, the damage can be calculated as:

$$D = 1 - \frac{\Delta L}{\Delta L^*}. \quad (16)$$

The results using equation (16) are shown in Fig. 13. The damage started from zero, as it is always assumed, that at the beginning of the test the material is in its virgin state. It is shown that damage variable increased slightly, and then suddenly rose sharply at the failure point (sudden death). Since  $D_m$  is equal to  $1 - D$ , the curve of  $D$  versus number of cycles can be converted to  $D_m$  versus the number of cycles ( $N$ ). This new curve is shown in Fig. 14. Equation (3) (using its simple form in equation (5)) is then fitted to this curve in order to obtain the damage parameters  $A$  and  $\beta$ .

Several attempts to fit curve  $N$  versus  $D_m$  directly have been unsuccessful. The reason is because there are not enough points near the failure point. Mathematically, the weight of the data is uneven. To overcome this problem, several points were

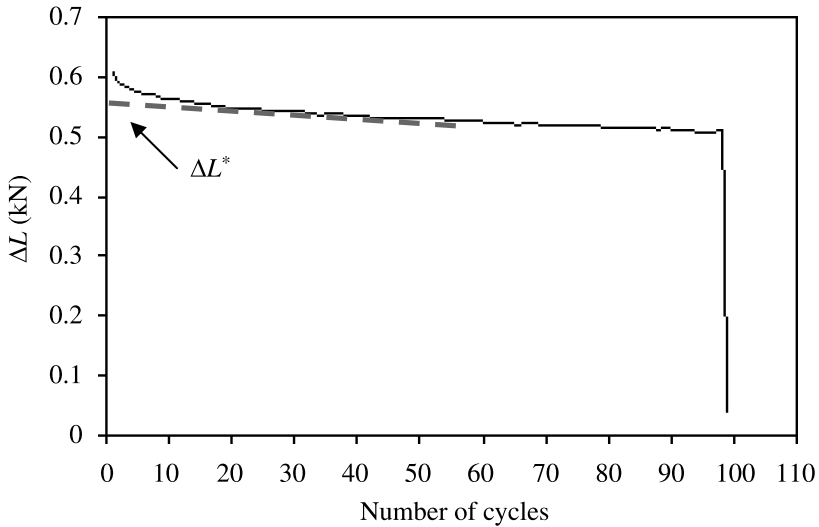


**Figure 12.** Load range,  $\Delta L$ , versus number of cycles for  $\Delta\sigma_{\text{eq}}^* = 43.88$  MPa.

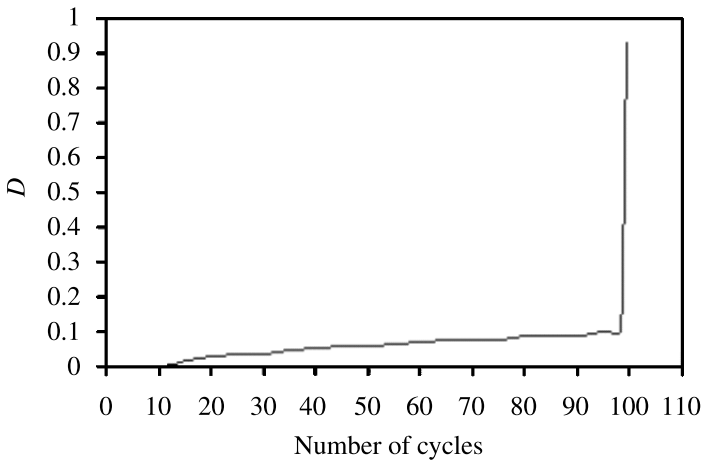


**Figure 13.** Damage value versus number of cycles for  $\Delta\sigma_{\text{eq}}^* = 43.88$  MPa.

added in-between the last and penultimate points as shown in Fig. 15. Adding these points is valid with the assumption that from the penultimate point to the last point, the change in  $D_m$  is linear.

After adding several points, the curve fitting process can be successfully performed. Figure 16 shows the fitted curve compared to the original data. Since the fitted curve is a continuous function, it is shown that damage variable has increased smoothly near the failure point (the last point). From the fitting process, two parameters were found:  $K_1 = 98.8$  and  $C_2 = 13.26$  with 95% of confidence bounds. The

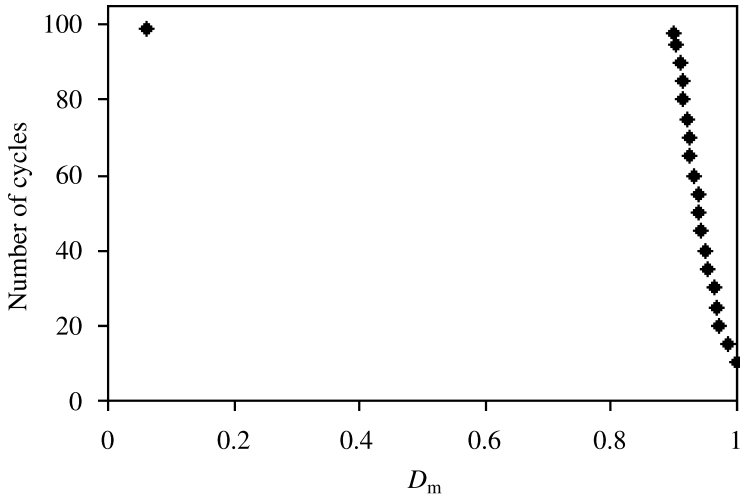


Figure 14. Number of cycles as a function of  $D_m$  for  $\Delta\sigma_{eq}^* = 43.88$  MPa.

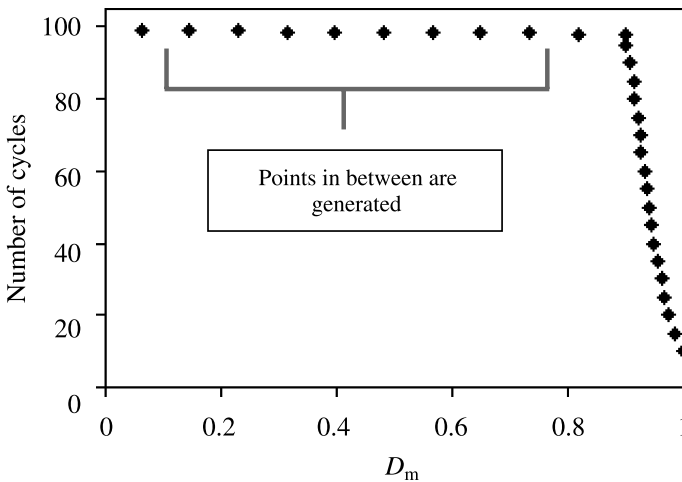


Figure 15. Number of cycles as a function of  $D_m$  with generated points for  $\Delta\sigma_{eq}^* = 43.88$  MPa.

quality of the fit is as follows: SSE (the sum of squared errors (residuals)) = 354.2; R-square (the ratio of the sum of squares of the regression (SSR) and the total sum of squares (SST)) = 0.9867; adjusted R-square (adjustment based on the residual degrees of freedom) = 0.9862; and RMSE (root mean squared error) = 3.622. After  $K_1$  and  $C_2$  were found, the damage parameters  $A$  and  $\beta$  were calculated and found to be:  $A = 6.01 \times 10^{-20}$ ;  $\beta = 9.391$ . With the same technique,  $A$  and  $\beta$  for different  $\Delta\sigma_{eq}^*$  (von-Mises stress range at the stabilized hardened state or at the undamaged state) have been calculated and listed in Table 1. Plots of  $A$  and  $\beta$  versus  $\Delta\sigma_{eq}^*$  are shown in Figs 17 and 18, respectively. From both figures, it is

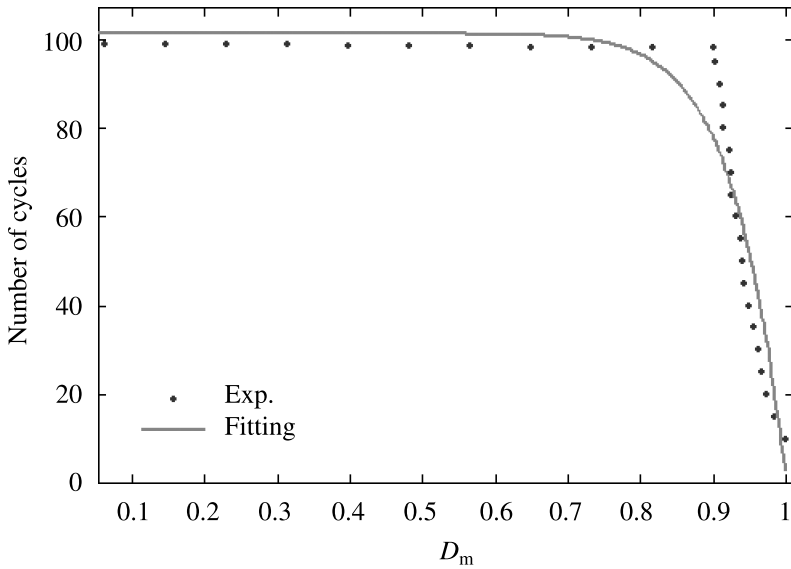


Figure 16. Fitted curve compared to experimental data for  $\Delta\sigma_{eq}^* = 43.88$  MPa.

Table 1.

Damage parameters  $A$  and  $\beta$  for different range of von-Mises stress at stabilization of hardening ( $\Delta\sigma_{eq}^*$ )

$\Delta\text{disp.}$ (mm)	$\Delta\sigma_{eq}^*$ (MPa)	$N_f$	$K_1$	$C_2$	$\beta$	$C_1$	$A$
1.40	44.18	10	9.724	11.76	10.68	$1.03 \times 10^{-1}$	$1.73 \times 10^{-20}$
1.29	43.88	99	101.3	13.79	12.71	$9.87 \times 10^{-3}$	$7.08 \times 10^{-25}$
1.11	43.15	179	181.5	15.75	14.67	$5.51 \times 10^{-3}$	$2.68 \times 10^{-28}$
1.09	41.94	418	424.4	14.74	13.66	$2.36 \times 10^{-3}$	$8.11 \times 10^{-27}$
0.92	34.6	9401	9557	26.39	25.31	$1.05 \times 10^{-4}$	$3.32 \times 10^{-45}$

shown that  $A$  has tendency to decrease, while  $\beta$  to increase. Finally, the damage from experiments (calculated by using equation (9)) is compared to the damage from prediction (plotted by using equation (3)) in Fig. 19. For other tests, using the same procedures (for different  $\Delta\sigma_{eq}^*$ ), different values of  $A$  and  $\beta$  have been found. The predicted damage curves are compared to the experimental damage curves in Fig. 20.

Fatigue tests with higher cycles to failure ( $N_f > 10000$  cycles) were performed. The damage evolution law could not be fitted to the damage experimental curves because the fitting process failed to converge. The highest number of cycles to failure, for which the fitting process converged, was  $N_f = 9401$ .

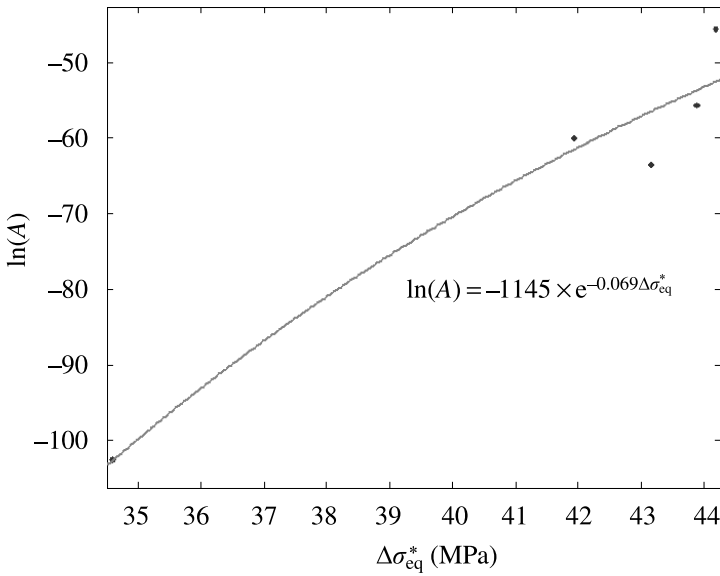


Figure 17. Damage parameter,  $\ln(A)$ , versus stress range  $\Delta\sigma_{eq}^*$ .

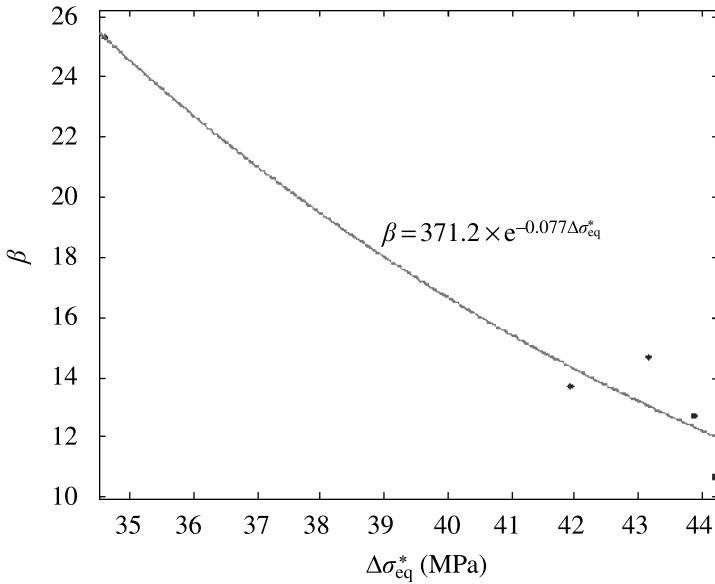


Figure 18. Damage parameter,  $\beta$ , versus stress range  $\Delta\sigma_{eq}^*$ .

#### 4. Conclusions

From the application of fatigue crack initiation damage evolution law to bulk adhesive test specimens, the following conclusions have been made:

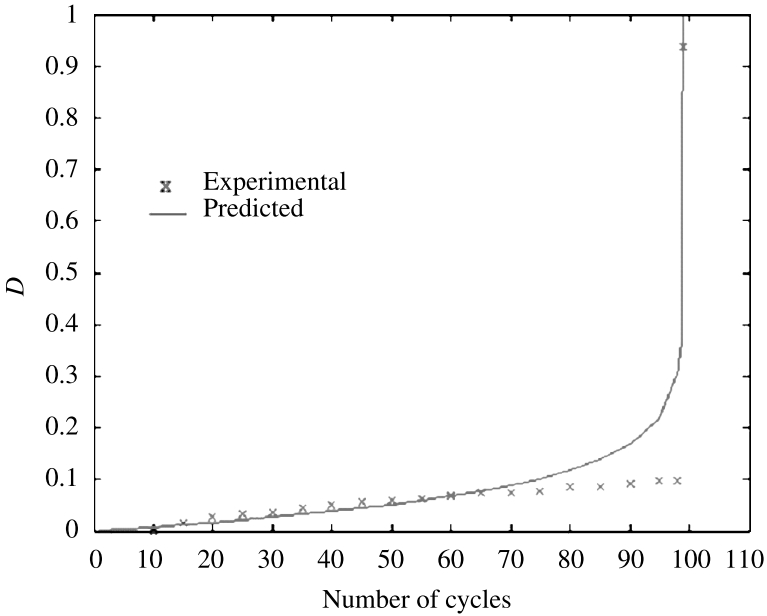


Figure 19. Damage value; experimental and predicted values for  $\Delta\sigma_{eq}^* = 43.88$  MPa.

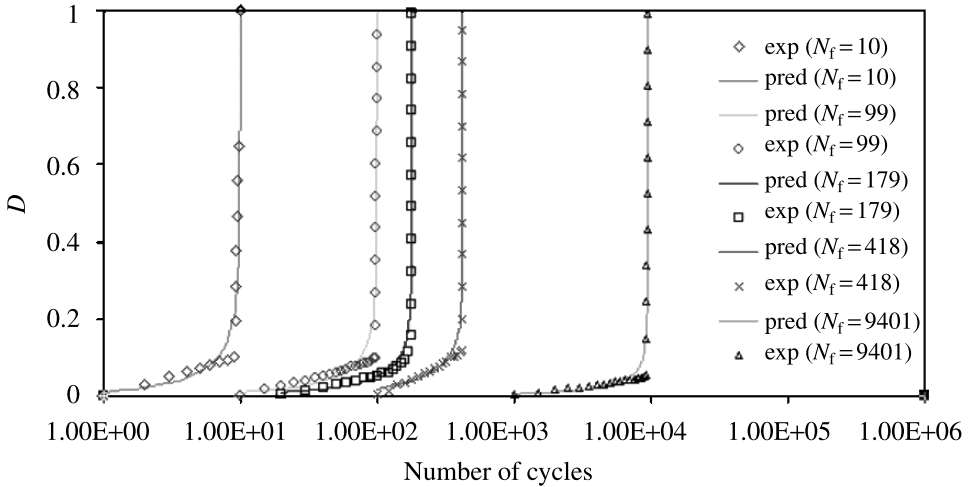


Figure 20. Comparison between experimental and predicted damage variables for all load range levels.

1. Bulk adhesive was suitable for initial determination of damage parameters, where triaxiality function is equal to one;
2. The damage parameters have been successfully extracted from the experimental data though curve fitting using the damage evolution law;

3. Additional data have been inserted into the damage curve for fitting process of damage evolution curve without changing its physical meaning. The aim was to weight the data near the failure point so that the fitting process could converge;
4. A procedure to obtain the damage parameters  $A$  and  $\beta$  of bulk adhesive has been proposed. With this procedure, the damage curve for different stress levels could be predicted. The fitting process only converges for low cycle fatigue failure, in these cases less than 10 000 cycles. Since the experimental tests were performed on bulk adhesive specimens, the applicability of low cycle fatigue may be limited to 10 000 cycles. However, since structural adhesive joints contain stress singularity points, low cycle fatigue damage model is always suitable for adhesive joints regardless of the number of cycles to failure because the stresses exceed the elastic limit and plastic zones take place around these singularity points.

Further application of the technique to adhesive in joints will be presented in part 2 of this paper, where multi-axial stress state and triaxiality function are considered in more details.

## References

1. S. K. Mazumdar, *Composite Manufacturing: Materials, Product and Process Engineering*. CRC Press (2002).
2. S. P. Timoshenko, *History of Strength of Materials*. Donner Publication (1982).
3. R. Blaum, *August Wöhler in Beiträge zur Geschichte der Technik und Industrie* **8**, 33 (1918).
4. J. Lemaitre and R. Desmorat, *Engineering Damage Mechanics*. Springer Verlag (2005).
5. V. M. Radhakrishnan, *On Bilinearity of Manson–Coffin Low Cycle Fatigue Relationship*, NASA Technical Memorandum 105840, October (1992).
6. J. Lemaitre and J. L. Chaboche, *Mechanics of Solid Materials*. Cambridge University Press (1998).
7. R. S. Courta, M. P. F. Sutcliffe and S. M. Tavakoli, *Int. J. Adhesion Adhesives* **21**, 455 (2001).
8. J. A. Harris and P. A. Fay, *Int. J. Adhesion Adhesives* **12**, 9 (1992).
9. Z. Zhang, J. K. Shang and F. V. Lawrence, *J. Adhesion* **49**, 23 (1995).
10. M. Imanaka, K. Haraga and T. Nishikawa, *J. Adhesion* **49**, 197 (1995).
11. A. D. Crocombe, C. Y. Ong, C. M. Chan, M. M. Abdel Wahab and I. A. Ashcroft, *J. Adhesion* **78**, 745 (2002).
12. V. Marcadon, Y. Nadot, A. Roy and J. L. Gacougnolle, *Int. J. Adhesion Adhesives* **26**, 481 (2006).
13. A. D. Crocombe, in: *Proceedings of Structural Adhesives in Engineering V (SAE V)*. Bristol: Institute of Materials, p. 80 (1998).
14. A. J. Curley, H. Hadavinia, A. J. Kinloch and A. C. Taylor, *Int. J. Fract.* **103**, 41 (2000).
15. G. Dean and B. Duncan, *Preparation and Testing of Bulk Specimens of Adhesives*. NPL Measurement Good Practice Guide No 17 (1998).
16. L. F. M. da Silva, R. D. Adams and M. Gibbs, *Int. J. Adhesion Adhesives* **24**, 69 (2003).
17. User Manual, Instron 5500R frame 6025 (1992).
18. W. Ramberg and W. R. Osgood, *Description of Stress–Strain Curves by Three Parameters. Technical Note No. 902*. National Advisory Committee For Aeronautics, Washington, DC (1943).

19. M. M. Abdel Wahab, I. A. Ashcroft, A. D. Crocombe and S. J. Shaw, *J. Adhesion Sci. Technol.* **15**, 763 (2001).
20. G. Z. Voyiadjis and P. I. Kattan, *Advances in Damage Mechanics: Metals and Metals Matrix Composites*. Elsevier, Oxford (1999).
21. User Guide, MATLAB ver. 7.1, Mathworks Inc. (2004).

## Appendix A

MATLAB Code for curve fitting of damage model to experimental data

```
function dm10gen(Dm,N)
% DM10GEN Create plot of datasets and fits

% Set up figure to receive datasets and fits
f_ = clf;
figure(f_);
set(f_,'Units','Pixels','Position',[318 115 680 484]);
legh_ = []; legt_ = {}; % handles and text for legend
xlim_ = [Inf - Inf]; % limits of x axis
ax_ = axes;
set(ax_,'Units','normalized','OuterPosition',[0 0 1 1]);
set(ax_,'Box','on');
axes(ax_); hold on;

% --- Plot data originally in dataset "N vs. Dm"
Dm = Dm(:);
N = N(:);
h_ = line(Dm,N,'Parent',ax_,'Color',[0.333333 0 0.666667],...
'LineStyle','none','LineWidth',1,...
'Marker','.', 'MarkerSize',12);
xlim_(1) = min(xlim_(1),min(Dm));
xlim_(2) = max(xlim_(2),max(Dm));
legh_(end + 1) = h_;
legt_{end + 1} = 'N vs. Dm';

% Nudge axis limits beyond data limits
if all(isfinite(xlim_))
    xlim_ = xlim_ + [-1 1] * 0.01 * diff(xlim_);
    set(ax_,'XLim',xlim_)
end

% --- Create fit "fit 1"
ok_ = ~(isnan(Dm) | isnan(N));
st_ = [0.07674199847374 0.5974476859008];
ft_ = fitype('k1 - k1 * x^k2',...
```

```

    'dependent', {'y'}, 'independent', {'x'}, ...
    'coefficients', {'k1', 'k2'});
% Fit this model using new data
cf_ = fit(Dm(ok_), N(ok_), ft_, 'Startpoint', st_);

% Or use coefficients from the original fit:
if 0
    cv_ = {9.724102351622, 11.75744857267};
    cf_ = cfit(ft_, cv_{:});
end

% Plot this fit
h_ = plot(cf_, 'fit', 0.95);
legend off; % turn off legend from plot method call
set(h_(1), 'Color', [100], ...
    'LineStyle', '-', 'LineWidth', 2, ...
    'Marker', 'none', 'MarkerSize', 6);
legh_(end + 1) = h_(1);
legt_{end + 1} = 'fit 1';

% Done plotting data and fits. Now finish up loose ends.
hold off;
h_ = legend(ax_, legh_, legt_, 'Location', 'NorthEast');
set(h_, 'Interpreter', 'none');
xlabel(ax_, ''); % remove x label
ylabel(ax_, ''); % remove y label

```

Copyright of Journal of Adhesion Science & Technology is the property of VSP International Science Publishers and its content may not be copied or emailed to multiple sites or posted to a listserv without the copyright holder's express written permission. However, users may print, download, or email articles for individual use.